SSRG International Journal of Mechanical Engineering
ISSN: 2348-8360/ https://doi.org/10.14445/23488360/IJME-V12I2P107

Volume 12 Issue 2, 75-87, February 2025

Original Article

Revolutionizing Solar Energy: Optimizing Thermal Performance of Flat Plate Solar Collectors with SiC Nanofluids

A. Rafi[1], S. Muthuvel[2]

[1,2]*Mechanical Engineering, Kalasalingam Academy of Research and Education, Tamil Nadu, India.*

[1]*Corresponding Author : rafi.a.321@outlook.com*

Received: 12 December 2024 Revised: 11 January 2025 Accepted: 10 February 2025 Published: 25 February 2025

Abstract *- The inefficiency of heat transfer devices is primarily due to using conventional fluids with poor heat transfer characteristics. Significant enhancements in thermal performance have been observed when these fluids are replaced with Nanofluids (NFs), which exhibit superior heat transfer and thermal conductivity properties. This research evaluates the efficiency of Silicon Carbide (SiC) NFs in a Flat Plate Solar Collector (FPSC) to enhance heat transfer performance. SiC nanoparticles, characterized by a cubic shape and 40–70 nm average size, were synthesized and dispersed in water at varying volume fractions (0.025%, 0.05%, 0.075%, and 0.1%). Their thermophysical properties were analyzed to confirm structural integrity and stability. Thermal conductivity measurements indicated significant improvements, with a maximum increase of 31.3% at 70°C for the highest volume fraction. Viscosity evaluations revealed that dynamic viscosity increased as temperature decreased, highlighting improved flow properties at higher temperatures. Experimental investigations were conducted in Coimbatore, India, following ASHRAE Standard 93-2003, to assess the FPSC's thermal performance under different conditions. The results demonstrated that adding SiC NFs significantly enhanced collector performance, achieving a peak thermal efficiency of 0.7496 at a 0.1% volume fraction with a mass flow rate of 0.033 kg/s, compared to a maximum efficiency of 0.558 when using water. These findings confirm that integrating SiC NFs in FPSCs leads to notable improvements in thermal efficiency, thereby contributing to advancements in solar thermal technology.*

Keywords *- SiC nanofluids, FPSC, Thermal efficiency, Renewable energy, Solar collectors, Heat transfer.*

1. Introduction

The economies of developing countries are experiencing significant growth in energy demand. The increase in world population plays a major role in increasing energy demand [1]. Fossil fuel resources are widely used to satisfy the current energy demands. The environmental pollution due to fossil fuels and their sustainability for future generations have raised critical concerns regarding power generation and utilization. Subsequently, renewable energy sources like solar energy become a viable long-term alternative to conventional energy systems [2]. Solar Photovoltaic (PV) cells convert the incoming solar radiation into electricity to meet power requirements. A solar collector captures incoming solar radiation, converts it into thermal energy, and distributes this heat to the working fluid circulating throughout the whole system to utilize in industrial applications [3].

Solar thermal collectors can be divided into two primary classes. Non-concentrating devices, like FPSC and evacuated tube collectors, utilize a wide surface area to directly collect sunlight without concentration, making them suitable for domestic and small-scale heating applications. Flat-plate solar collectors comprise a flat absorber surface, a transparent cover, and an insulating material that effectively captures solar radiation to increase the temperature of a fluid [4]. Conversely, concentrating systems, such as parabolic troughs and solar power towers, employ mirrors or lenses to focus sunlight onto a confined zone. This concentrated energy is utilized to produce high temperatures appropriate for industrial applications and electricity generation.

FPSCs are widely used in applications such as residential and commercial water heating. When sunlight reaches the collector, a huge amount of energy is absorbed by the plate and is then transferred to the liquid circulating inside the tubes, which then transfers the energy to the storage system [5]. The thermal efficiency of FPSC is crucial for heat exchangers. The poor thermal conductivity of conventional working fluids like water, ethylene glycol, and transformer oil limits the heat transfer capability. Nanofluids are fluids with suspended nanoparticles that enhance heat transfer

properties, making them highly effective alternatives to conventional fluids. Their significantly improved thermal conductivity allows for better heat absorption and transfer, directly influencing FPSC efficiency and overall thermal performance [6]. These innovations allow better heat absorption and transfer, improving thermal efficiency. Despite extensive studies on improving the thermal performance of FPSCs using NFs, the application of SiC nanofluids remains underexplored. While studies have examined metal oxide and carbon-based nanofluids, limited attention has been given to SiC, which offers high thermal conductivity, chemical stability, and excellent dispersion in base fluids. The lack of experimental validation for SiC nanofluids in FPSCs creates a significant research gap in assessing their practical efficiency. This study addresses this limitation by investigating the thermal performance of SiC nanofluids at varying volume fractions, providing a novel comparative analysis against conventional fluids to establish their potential for enhancing solar thermal applications. The major contributions of the study are listed below.

- To examine the stability of the prepared SiC NF.
- To assess the thermal feasibility of SiC NFs.
- To enhance the heat transfer efficiency in solar thermal applications.
- To assess the energy productivity of the solar collector under varying situations.

The rest of the paper is organized as follows: Section 2 presents a literature review, underscoring the necessity of this research. Section 3 describes the preparation process and experimental procedures used to evaluate the performance of NFs in FPSC. Section 4 discusses the results, emphasizing the effectiveness of the proposed model. Finally, Section 5 concludes the study by summarizing its key contributions.

2. Literature Review

Husseın et al. [7] evaluated the thermal capacity of CuO/H_2O NFs. The experiments were conducted under varying CuO concentrations and different mass flow rates in Iraqi weather conditions. The results demonstrated a direct relation between the temperature and nanoparticle concentration. The 1% $CuO - H_2O$ NF achieved a 32% rise in collector thermal effectiveness, outperforming pure water by 11.3%. The increase in output power due to the increasing mass flow rate was limited by the concentrations of nanoparticles. Farhana et al. [8] explored the efficiency of FPSC using Al_2O_3 and Crystal Nanocellulose (CNC) NFs. The thermophysical characteristics of NFs were evaluated to analyze their characteristics and stability. Results showed that employing 0.5% Al_2O_3 and 0.5% CNC NFs improved efficiency by up to 2.48% and 8.46%, respectively. The study possessed challenges, including the mechanical instability of CNC NF.

Hawwash et al. [9] considered the thermal feasibility of using copper oxide-water and alumina oxide-water NFs. A validated Computational Fluid Dynamics (CFD) model was employed, and the outcomes showed a rise in pressure drop with improved thermal efficiency. The CuO NFs with 0.5% volume fraction achieved the highest efficiency, outperforming alumina oxide NFs. The study was limited by uncertainty regarding fluid characteristics and heat transfer mechanisms. Zarda et al. [10] considered the thermal performance of FPSC by means of diamond/H_2O NFs. Different concentrations of nanoparticles were subjected to numerical analysis and validated with existing experimental data. Simulations were conducted using ANSYS/FLUENT software to model Iraq's climatic conditions, where solar intensity diminishes after midday, impacting temperature and collector competence. The maximum thermal productivity attained was 68.90% with a 1% diamond/water NF, representing a notable 12.2% enhancement compared to pure water. The study was limited by the long-term stability of NFs and the limited range of nanoparticle concentrations.

Akram et al. [11] created water-based NFs using covalently functionalized carbon nanoplatelets (f-GNPs) and surfactant-treated metal oxide nanoparticles (ZnO and SiO_2), with stability verified using UV-vis spectroscopy for 60 days (f-GNPs) and 30 days (metal oxides). Experimental evaluations demonstrated enhanced thermal properties relative to distilled water. Evaluations of an FPSC revealed a thermal efficiency improvement of up to 17.45% for f-GNPs at a flow rate of 1.6 kg/min as compared to water. Bharadwaj [12] conducted a study with a hybrid NF composed of Al_2O_3 and TiO_2 in FPSC to improve thermal efficiency. NFs with particle sizes between 30-50 nm and concentrations from 0.25% to 1% were evaluated, attaining a maximum efficacy of 62% at a 0.75% volume concentration. The study used controlled testing in FPSC setups to evaluate thermal efficiency at various concentrations and flow rates, with optimal performance observed at a 0.75% volume concentration and a 1.25 L/min flow rate. Limitations included scaling issues and the long-term stability of NFs in practical applications of FPSC.

Aghili Yegane et al. [13] evaluated the thermal performance of FPSC by means of hybrid NFs. The study explored the porous media within the collector channels and employed the Darcy-Brinkman model to analyze flow behavior. The results indicated that the hybrid combination of copper and alumina showed enhanced efficiencies. However, the study was limited by the sensitivity of collector performance. Balam et al. [14] developed a fourth-order non-dimensional transient numerical method to enhance the accuracy of thermal efficiency. The study highlighted the impact of flow mode transitions on convection heat transfer. However, the high grid density required to resolve the flow led to increased computational costs.

Shafiq et al. [15] evaluated the FPSC performance with Fe_3O_4-water NF concerning the thermohydraulic

characteristics having various operating parameters. The findings demonstrated an increased volume fraction with an improved exergy efficiency of 8.90%. The optimal volume fraction was observed using the performance index criteria. The numerical modeling faced limitations related to grid resolution and convergence. Ajeena et al. [16] developed a hybrid NF using ZrO_2-SiC particles in distilled water. The results demonstrated enhanced exergy and energy efficiencies in the presence of NF. There was an increase of 31.64% in thermal efficiency. The narrow operation range limits its applicability to other NF concentrations.

He et al. [17] investigated FPSC thermal performance optimization by analyzing environmental conditions, operational parameters, and structural dimensions. Numerical simulations were used to optimize microchannel configurations, while experimental tests validated mathematical models on stainless steel FPSCs. Results showed that increasing microchannel width and corrugation height improved heat transfer, achieving a projected momentary efficiency of 86.10%. A mathematical model established the relationship between efficiency and surrounding conditions. The use of stainless steel enhanced durability and temperature uniformity. However, limitations included airflow distribution complexities, leading to pressure losses that impacted efficiency. Future studies were recommended to refine microchannel designs and optimize fluid flow.

The current research on Nanofluids (NFs) in Flat Plate Solar Collectors (FPSC) reveals several key problems that need addressing. First, there is a lack of optimization in nanoparticle concentration and size, which is crucial for achieving the highest thermal performance while maintaining stability. Many studies also face challenges regarding the long-term stability and durability of NFs, particularly when exposed to varying environmental conditions, leading to concerns about their reliability in real-world applications. Additionally, there is limited investigation into NF-based systems' economic feasibility and scalability compared to conventional solar collectors, which is essential for practical implementation. The integration of new nanomaterials and synthesis methods has been underexplored despite their potential to improve both the sustainability and performance of FPSC systems. Lastly, many studies fail to address the complexities related to fluid flow distribution, pressure losses, and the impact of system design on overall efficiency, indicating a need for further research to optimize both thermal and hydraulic performance.

3. Materials and Methods

The performance of SiC NF-based FPSC was investigated in this study by conducting systematic evaluations. The thermophysical properties of SiC NF were analyzed to regulate the optimal concentration for enhanced heat transfer. The collector's energy performance was evaluated under several operational situations, emphasizing aspects such as inlet temperature, flow rate, and sun irradiation. Extensive experimentation was provided by numerical simulations to explore the heat transfer dynamics in the collector. The gathered data were examined to assess the solar collector system's effectiveness and total energy production, facilitating an inclusive understanding of the advantages of incorporating SiC NFs in solar thermal applications.

3.1. Preparation of Study Material

The nanoparticle material of SiC in the form of powder with a cubic shape having 99% purity and a 40-70 nm average diameter is utilized for this study. SiC NFs are prepared by integrating silicon carbide nanoparticles into water due to their properties like nontoxicity, nonflammability, high stability in water, and being environmentally friendly. Table 1 tabulates the physical properties of the silicon carbide nanoparticle.

Table 1. Thermophysical characteristics of SiC

Properties	Silicon Carbide
Chemical formula	SiC
Morphology	Cubic structure
Color	Grayish white
Particle size	40-70 nm
Thermal conductivity	330 W/m-K
Specific heat	690 J/kg-K
Specific Surface Area	10-75 m2g
Density	3.2 g/cm3
Thermal expansion	4.3µm/m-K

The SiC/H_2O was prepared using two steps for mixing the nanoparticles and the base liquid. Initially, the SiC nanoparticles were weighed by a precision balance, and a specified mass for the study was dispersed into the H_2O. The mechanical mixing was done using a magnetic stirrer to guarantee uniform distribution of nanoparticles. An ultrasonic homogenizer was used for ultrasonic agitation for 90 minutes to reduce particle agglomeration. The ultrasonic energy improved the colloidal stability of the NF by inhibiting particle aggregation. For the experimental analysis, the SiC/water NF was produced at four volume fractions of 0.025%, 0.05%, 0.075%, and 0.1%. A zeta potential analyzer was implemented to test the stability of the prepared NF.

3.2. Characterization of the NF

The characterization of the NF was analyzed by employing several analytical techniques. X-ray powder diffraction (XRD) at 1/min scan under 40 kV/30 mA defines the crystalline structure of the SiC nanoparticles. The cubic structure is confirmed through the observed diffraction peaks, as shown in Figure 1. Each peak in the pattern verified the presence of SiC nanoparticles. Using Fourier Transform Infrared (FTIR) spectroscopy, the chemical bonds and

surface functional groups were examined [18]. In Transmission Electron Microscopy (TEM), a thin film of the nanoparticle sample is prepared by allowing a high-energy stream of electrons to pass through it [19]. These transmitted electrons are captured by a phosphorescent screen situated behind the sample. Thus, the morphology and size distribution of the nanoparticle reveals the cubic shape ranging from 40 to 70 nm, as depicted in Figure (2). These analyses ensured the structural integrity, stability, and suitability of SiC nanofluids for heat transfer applications.

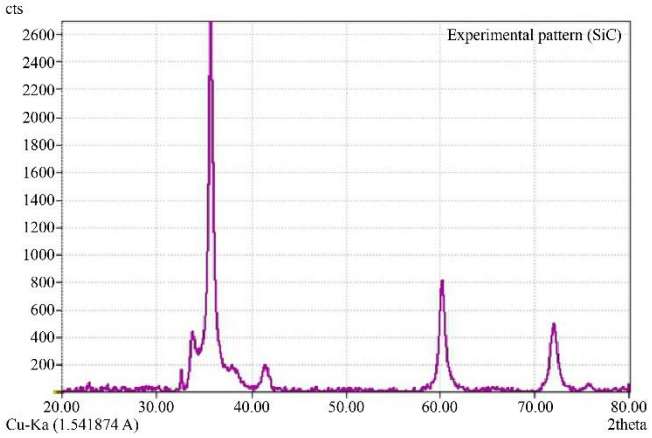

Fig. 1 SiC X-ray diffraction pattern

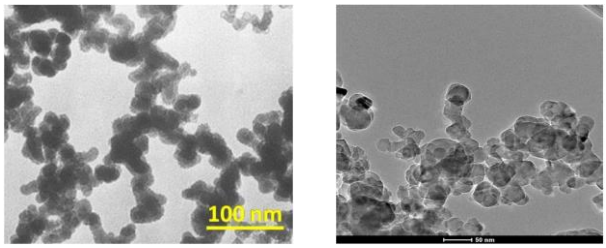

Fig. 2 TEM images of SiC particles

Equation (1) describes the calculation of the NF density.

$$\rho_{nf} = \rho_{np_1} \cdot \varphi_1 + \rho_{np_2} \cdot \varphi_2 + \rho_{bf} \cdot (1 - \varphi_1 - \varphi_2) \quad (1)$$

Where ρ_{nf} is the overall NF density, ρ_{np_1} and ρ_{np_2} are the densities of two nanoparticles. φ_1 and φ_1 are the volume fractions and ρ_{bf} is the base fluid density-weighted by the remaining volume fraction. Equation (2) expresses the specific heat capacity of the NF.

$$C_{p,nf} = C_{p,np_1} \cdot \varphi_1 + C_{p,np_2} \cdot \varphi_2 + \rho_{bf} \cdot C_{p,bf}(1 - \varphi_1 - \varphi_2) \quad (2)$$

Where $C_{p,bf}$ is the specific heat capacity of the NF.

3.3. Thermal Conductivity Measurement

The study examined the thermal conductivity of SiC NF in H_2O utilizing the Transient Hot-Wire (THW) method with a KD2-Pro device. This technique employs a thermal pulse applied to a thin wire sensor (KS-1) submerged in the NF, facilitating an accurate assessment of the material's thermal properties. The sensor, constructed from stainless steel having a 1.25 mm diameter and 70 mm length, was carefully oriented vertically at the center of a vial containing the NF sample to mitigate disturbances that could influence convective heat transmission.

The experiment was performed at SiC volume concentrations of 0.025%, 0.05%, 0.075%, and 0.1%. A temperature bath was employed to maintain a consistent temperature, ensuring precise thermal conductivity measurements during the testing process. Equation (3) uses Fourier's law of heat equation to determine the heat transmission from the wire to the surrounding fluid.

$$q = -k \cdot A \cdot \frac{dT}{dx} \quad (3)$$

Where A, k are the surface area and the thermal conductivity of the fluid, respectively, and $\frac{dT}{dx}$ is the temperature gradient. Equation (4) defines the rate of change of temperature in the fluid.

$$\frac{dT}{dt} = \frac{q}{m \cdot c} \quad (4)$$

Where m is the mass. Equation (5) provides the thermal conductivity based on the measured temperature response of the fluid.

$$k = \frac{q \cdot L}{\Delta T \cdot t} \quad (5)$$

Where L is the distance from the wire to the point of measurement, ΔT is the change in temperature of the fluid over the time t. The KD2-Pro device was calibrated utilizing a standard glycerol sample. The calibration was followed by measurements of pure water at different temperatures, comparing the results with values from the ASHRAE Handbook to validate the instrument's precision, as shown in Figure 3.

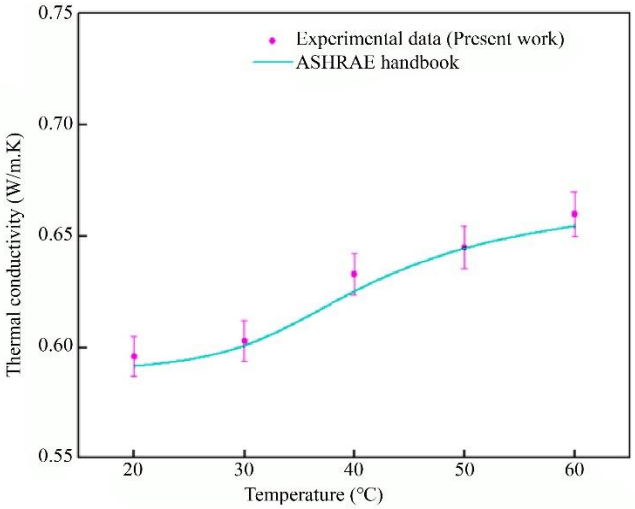

Fig. 3 Validation of thermal conductivity results of water with ASHRAE handbook

3.4. Viscosity Measurement

The dynamic viscosity of SiC/water was evaluated using a Brookfield DV2EXTRA-Pro rotational viscometer [20]. This device measures the shear resistance of fluid when a spindle is immersed in the NF. Equation (6) represents the dynamic viscosity of the fluid.

$$\mu = \frac{T}{\dot{\gamma}} \tag{6}$$

Where T, $\dot{\gamma}$ are the shear stress and shear rate, respectively. The viscometer was calibrated before the measurements using the base liquid at room temperature. A highly précised temperature bath in the range of 30^0C to 70^0C with increments of 10^0C was incorporated to ensure accurate viscosity measurements.

This allows us to analyze the impact of temperature on the viscosity of the NF. Equation (7) calculates the shear stress based on the spindle's geometry and the torque M applied.

$$\tau = \frac{M}{2\pi r^3} \tag{7}$$

Where r is the radius of the spindle. The shear rate for a rotational viscometer is given by Equation (8).

$$\dot{\gamma} = \frac{2\pi N}{60} \cdot \frac{1}{r} \tag{8}$$

Where N is the spindle rotational speed. The study employed a spindle with a shear rate coefficient of 1.325 alongside a small adapter device to ensure precise measurements. Thus, the dynamic viscosity in terms of torque and rotational speed is given by Equation (9).

$$\mu = \frac{M \cdot 60}{2\pi N \cdot r^3} \tag{9}$$

Equation (10) represents the effect of temperature on viscosity.

$$\mu(T) = Ae^{\frac{B}{T}} \tag{10}$$

Where A and B are the empirical constants, and T is the absolute temperature.

3.5. Experimental Setup

The experimental investigations on the FPSC were conducted at the Amritha University in Coimbatore, Tamil Nadu (Longitude 76.93°E, Latitude 11.02°N). The location was chosen to ensure maximum solar radiation exposure without any shadow intrusion. Coimbatore typically experiences solar radiation in the 4.8 to 6.5 kWh/m2/day range. The workflow of the proposed study is illustrated in Figure 4. The solar collector was positioned with its tilt angle and azimuth optimized for maximum energy capture. In the northern hemisphere, a southern orientation is optimal, and the best tilt angle for the solar collector is set at 13°, facilitating maximum daily solar radiation exposure. For testing, a 13° tilt angle was sustained, suitable for optimizing radiation absorption in this location, positioning the collector surface perpendicular to sun rays at noon.

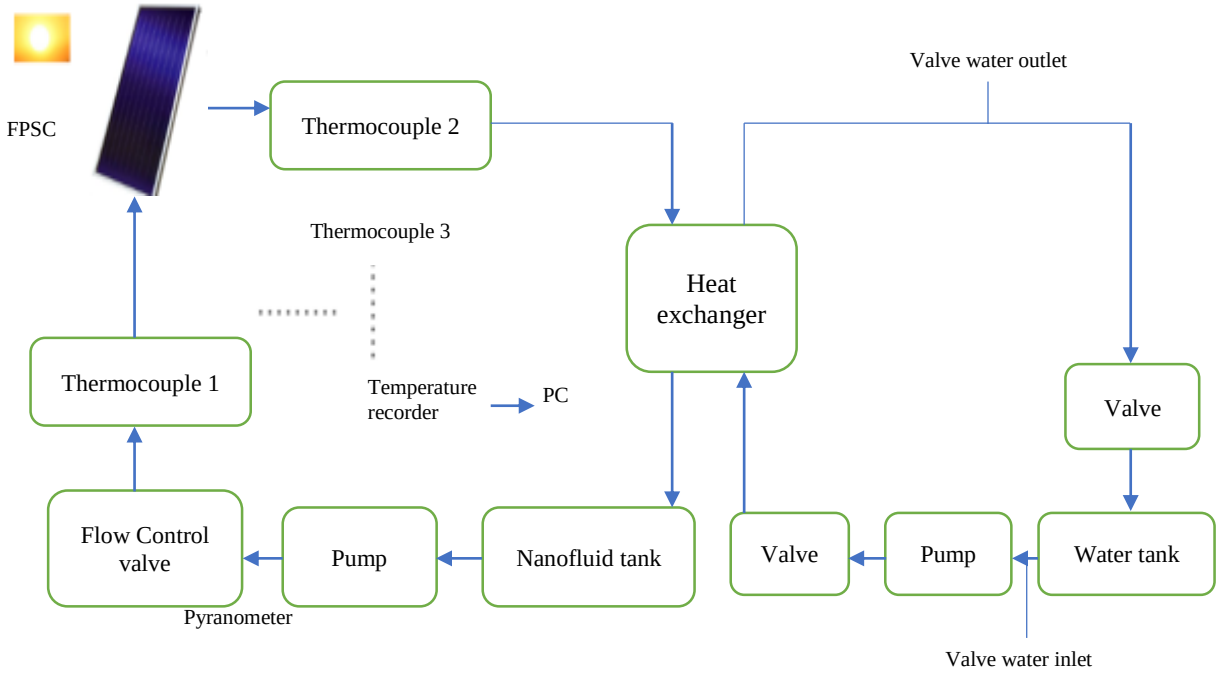

Fig. 4 Schematic representation of the experimental setup

The technical specifications of the FPSC arrangement and the instruments used in this study are tabulated in Tables 2 and 3, respectively.

Table 2. Specifications of FPSC

Parameters	Specifications
Collector size	2×1×0.15m
Collector tilt angle	130
Absorber plate thickness	0.00045 m
No. of riser pipes	7
Glass cover thickness	0.004 m
Insulation layer material	Glass wool
Thermal conductivity of the absorber plate	386 W/mK
Tube spacing between risers	0.095 m
Outer diameter of riser pipe	0.01 m
Inner diameter of riser piper	0.0095 m
Storage tank capacity	100 L
Heat exchanger type	ladder

Table 3. Specifications of instruments

Instruments	Values
Weighing Machine (Ace, Model-KD 200)	
Least Count	0.2 mg
Pyranometer (Kipp and Zonen, model CM4)	
Max. Solar Irradiance	4000 W/m^2
Field Range	180^0
6 Channel Data Loggers (TLOG Data Logger-Embuilt Technologies)	
Maximum Range	-10^0 C to +80^0 C
Thermocouple (K-Type)	
Range	-50 to 200^0 C
Accuracy	$\pm$0.1%

The pump circulates the NF and heats it within the solar collector. Upon heating, the NF leaves the collector and reaches the secondary loop via the heat exchanger, which is stored in a tank. Diverse instruments are utilized for measurement, including K-type thermocouples to monitor inlet and outlet fluid temperatures, in conjunction with a flow sensor to determine liquid flow. A fundamental valve is installed to control the flow rate. A pyranometer quantifies solar radiation, while an auxiliary thermocouple evaluates ambient temperature. The study employs a tank volume of around 100 litres. A flow sensor is positioned before the electric pump, and a simple valve is placed inside the arrangement following the pump to regulate the mass flow rate of the NF. Four K-type thermocouples monitor the outlet and inlet fluid temperatures, while one thermocouple measures the air temperature. A 6-channel data logger is linked to all sensors, and the measurement instruments, including the temperature data logger and pyranometer, connect to a PC for data acquisition. The calibration of devices was conducted before, during, and after the tests.

3.6. Testing Method

This study evaluated the productivity of the solar collector grounded on ASHRAE Standard 93-2003, which specifies testing methods for measuring the thermal feasibility of solar collectors [21]. The standard enables the assessment of instant efficacy values across several groupings of ambient temperature, inlet temperature, and incident solar radiation. Calculations and data processing were directed in accordance with the first law of thermodynamics, necessitating the experimental analysis of the rate of incident radiation from the sun and the energy imparted to the fluid as it traverses the collector, whether under quasi or steady conditions. In accordance with ASHRAE rules, trials were conducted at various inlet temperatures.

The studies were executed on sunny days from 10 a.m. to 4 p.m., segmented into six 60-minute intervals, each comprising 15-minute test sessions to maintain quasi-steady state conditions. Throughout the testing phases, the inlet and ambient temperatures exhibited stability, with variations of ±0.8°C and ±0.6°C, respectively. Solar radiation was measured utilizing a pyranometer, maintaining an irradiance threshold of no less than 790 W/m², with variations not exceeding ±32 W/m². Ambient temperature and wind speed were measured to ensure adherence to the specified range of 3 to 6 m/s. The system's working fluid, the NF, was pumped through the collection pipes. Mass flow rates of 0.0167, 0.025, and 0.033 kg/s were evaluated to determine thermal competence under different flow circumstances.

Before initiating data collection, the solar collector was subjected to daylight without fluid circulation until the internal fluid temperature was equilibrated with the inlet temperature. This phase was necessary for attaining steady-state situations. Following stabilization, the NF was circulated through the pipes for a minimum of 30 minutes before the initiation of data collection. Each test run starts after a 15-minute pre-data period, through which the collector system is observed to confirm steady-state conditions. Data was gathered at 5-minute intervals during the data collection period. Thermocouples recorded inlet, outlet, and ambient temperatures, while a pyranometer measured solar irradiation. All measurement instruments were calibrated before and after the testing to ensure precision. Equation (11) provides the useful heat gain energy from the solar collector.

$$Q_u = \dot{m} C_p (T_{fo} - T_{fi}) \tag{11}$$

The mass flow rate of the NF is represented by ṁ, while T_{fo} and T_{fi} denote the outlet and inlet temperatures,

respectively. The net solar energy absorbed by the collector is given by Equation (12).

$$Q_u = A_c F_r [G_t(\tau\alpha) - U_L(T_{fi} - T_a)] \quad (12)$$

Where A_c is the collector area, F_r is the heat removal factor, G_t represents the total incident radiation, τ is the transmittance, α is the absorptance of the collector, U_L is the overall heat loss coefficient, and T_a is the ambient temperature. The thermal efficiency of the FPSC is determined by the ratio of useful energy gained to the total energy input from solar radiation, as expressed in Equation (13).

$$\eta = \frac{Q_u}{A_c G_t}$$

$$= \frac{\dot{m} C_p (T_{fo} - T_{fi})}{A_c G_t} \quad (13)$$

Equation (14) demonstrates the reformulated efficiency equation, explaining the efficiency in terms of energy absorbed compared to energy lost.

$$\eta = F_R \left[\tau\alpha - U_L \left(\frac{T_{fi} - T_a}{G_t}\right)\right] \quad (14)$$

Where F_R is the heat removal factor as expressed by Equation (15).

$$F_R = \frac{\dot{m} C_p (T_{fo} - T_{fi})}{A_c [G_t(\tau\alpha) - U_L(T_{fi} - T_a)]} \quad (15)$$

4. Results and Discussion

4.1. SiC Nanoparticles Characterization

The examination of nanoparticle characteristics involves shape evaluation along with a comprehensive analysis of their topography, elemental composition, and morphology by Field Emission Scanning Electron Microscopy (FESEM).

The spatial compositional variations determine the surface contaminants and any fractures. FESEM is highly used for evaluating the consistency of nanoparticle morphologies and describing NFs, making it a crucial instrument for th1=-2korough nanoparticle examination.

Figure 5 demonstrates that the FESEM micrographs of SiC nanoparticles at magnifications of 200 nm and 1 µm have a characteristic cubic morphology. Moreover, energy-dispersive X-ray spectroscopy (EDX) enhances FESEM by identifying X-rays released from the sample to determine its elemental composition.

The EDX data illustrated in Figure 6 indicate the sample's composition, showing the presence of silicon and carbon with a major peak at around 1.75 keV, signifying good purity for the sample.

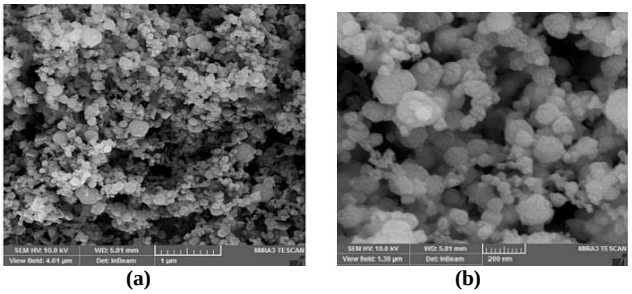

(a) **(b)**

Fig. 5 FESEM images of SiC nanoparticles (a) 1µm, and (b) 200 nm.

Fourier Transform Infrared Spectroscopy (FTIR) analyzes both the absorption and emission spectra of IR. The dimensions of the samples are determined by analyzing the vibrations of molecules and polyatomic ions. Molecular vibrations are classified into flexural and tensile types, and tensile types are subdivided into asymmetric and symmetric variations. The first half-cycle creates a dipole moment in asymmetric tensile vibrations, while the subsequent half-cycle produces opposing bipolar motions. Molecular vibrations produce distinct vibrational frequencies that alter dipole moments, leading the molecule to enter the infrared absorption spectrum. Figure 7 displays the FTIR spectra of the nanoparticles.

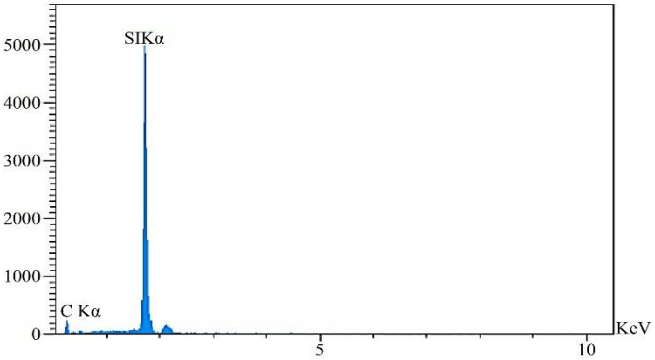

Fig. 6 EDX of SiC

The stability of the synthesized NF was determined using a zeta potential analyzer. Figure 8 illustrates the stability analysis of SiC NFs, where the zeta potential value over ±30 mV indicated good stability. This value ensures that nanoparticles are well-distributed within the base fluid without further sedimentation over time.

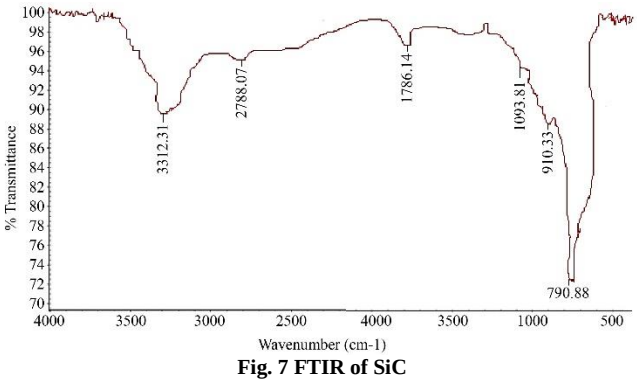

Fig. 7 FTIR of SiC

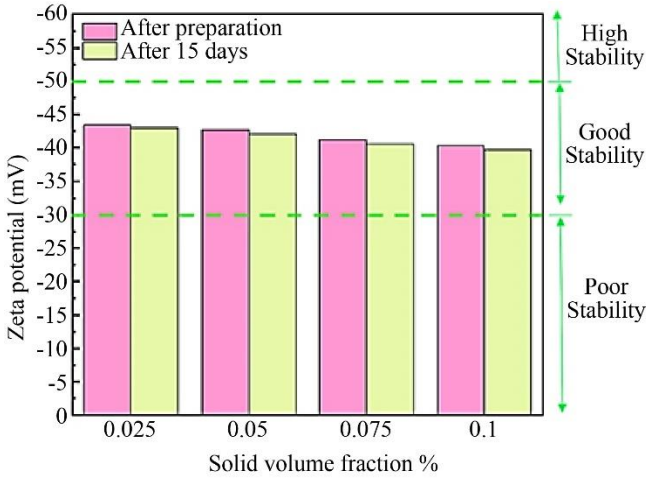

Fig. 8 SiC stability analysis

4.2. Analysis of Thermal Conductivity

With the rise in temperature and SiC nanoparticle concentration, there was a corresponding increase in thermal conductivity. The connection between the thermal conductivity and varying volume fractions of the nanoparticle is illustrated in Figure 9. At 40 °C, thermal conductivity increases by 8.33%, 13.23%, 18.73%, and 23.33% for volume fractions of 0.025%, 0.05%, 0.075%, and 0.1% of SiC, respectively, relative to pure water. The clustering of nanoparticles enhanced Brownian motion, and the formation of layers between the nanoparticles and the fluids is responsible for this rise in thermal conductivity. As the volume fraction increases, the frequency of particle collisions increases, enhancing the thermal conductivity of the NF. Higher temperatures also significantly enhance conductivity, with increases of nearly 19.18%, 20.06%, 26.67%, and 31.3% for 0.025%, 0.05%, 0.075%, and 0.1% SiC at 70 °C. Elevated temperatures increase the frequency of particle collisions, improving heat transfer and thermal conductivity.

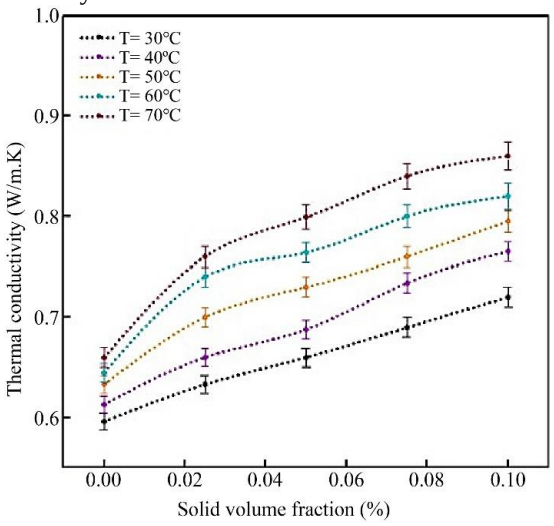

Fig. 9 Thermal conductivity of SiC NF

4.3. Dynamic Viscosity Analysis

The presence of SiC particles influences the dynamic viscosity of the NF, as illustrated in Figure 10. A rise in dynamic viscosity was experienced with decreasing temperature. At 40 °C, dynamic viscosity improved by 22.5%, 45.00%, 71.25%, and 91.13% for SiC volume fractions of 0.025%, 0.05%, 0.075%, and 0.1%, respectively, compared to water.

As temperature decreases, the adhesive forces between particles increase, resulting in an increase in viscosity. Conversely, as the temperature rises, viscosity consistently reduces for each examined volume fraction. At 70 °C, viscosity reductions of 45.46%, 47.8%, 38.6%, and 30.67% were observed for SiC volume fractions of 0.025%, 0.05%, 0.075%, and 0.1%, respectively, compared to the SiC/water NF at 30°C.

Increased temperature reduces resistance among fluid layers, which decreases viscosity. Heating the liquid weakens intermolecular interactions, resulting in increased collisions among nanoparticles and Brownian motion within the NF.

The enhanced thermal conductivity and decreased viscosity at higher temperatures suggest that the NF has higher heat transfer efficiency relative to the base fluid. This leads to reduced viscosity during thermal exchange in solar collectors.

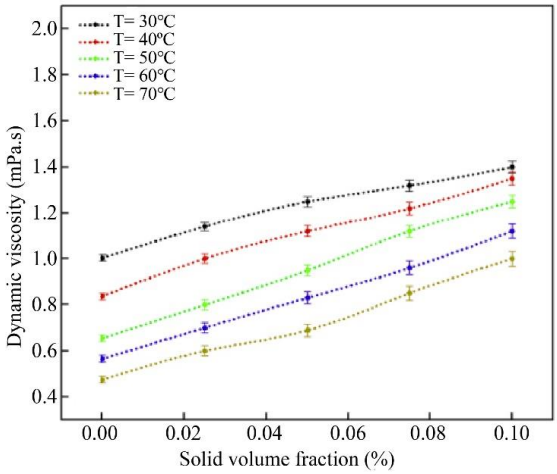

Fig. 10 Dynamic viscosity of SiC

4.4. Thermal Performance Analysis of the FPSC

The study examined the thermal performance of the collector concerning the decreased [(Ti-Ta)/GT] temperature parameter as an independent factor across several scenarios.

Using ASHRAE standards, a linear regression was applied to establish a relationship between reduced temperature and thermal efficiency, and the slope of this line denotes the $F_r U_L$ removed energy parameters.

When [(Ti-Ta)/GT] equals zero, the point where the line intersects the y-axis is known as the absorbed energy parameter. At this condition, the thermal efficiency reaches its maximum, highlighting the thermo-optical properties of the system. The study examined the effects of diverse volume fractions and mass flow rates of the nanoparticles.

This study investigated the impact of different nanoparticle volume fractions of SiC NF. Figure 11 illustrates the correlation between thermal efficiency and the [(Ti-Ta)/GT] for H_2O and the corresponding NF at mass flow rates of 0.0167, 0.0250, and 0.033 kg/s.

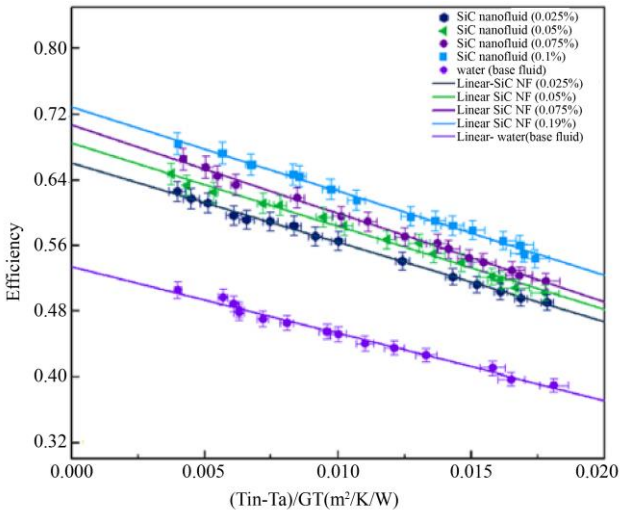

(a) 0.0167 kg/s

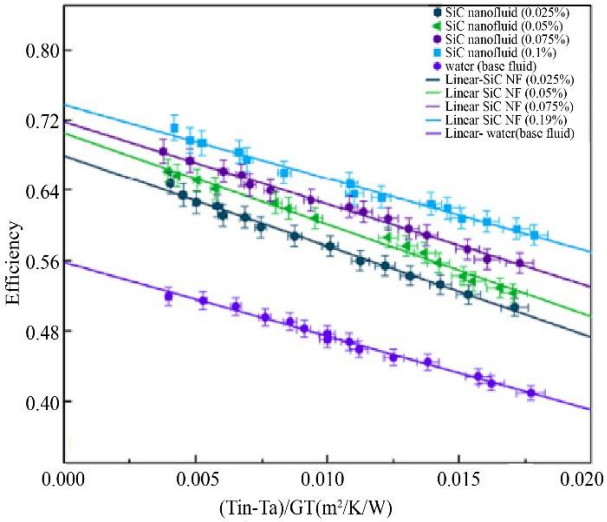

(b) 0.0250 kg/s

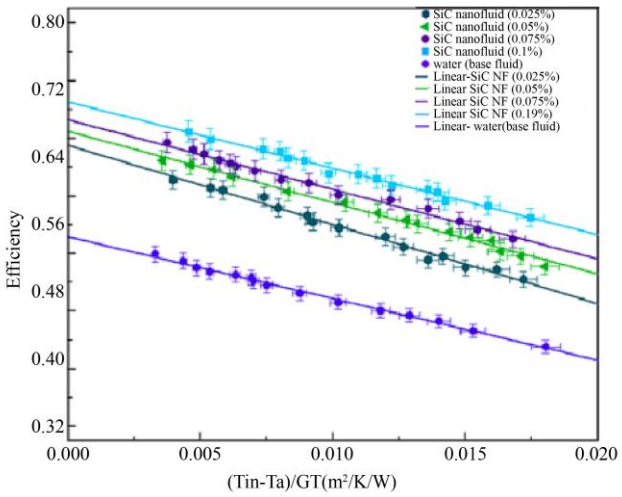

(c) 0.033 kg/s

Fig. 11 Thermal efficiency of FPSC for SiC-water NF

Table 4 shows the performance metrics of SiC NF and water in a solar collector. The improved mass flow rates improve the thermal characteristics of the collector. The peak performance recorded under all conditions attained a maximum efficacy of 0.7496 at the highest mass flow rate and volume fraction. This study examines the impact of different volume fractions of SiC nanoparticles in NF on the effectiveness of a solar collector. The results confirmed that increasing the volume fraction improves the system's efficiency.

At a 0.025% volume fraction, a mass flow rate of 0.0167 kg/s yields an absorbed energy parameter. F_r (τα) of 0.638, which increases to 0.6751 at 0.0330 kg/s. A 0.05% volume fraction shows comparable performance, increasing efficiencies from 0.669 at 0.0167 kg/s to 0.7061 at 0.0330 kg/s. The 0.075% volume fraction improves performance, reaching a maximum of 0.7259 at 0.0330 kg/s. At 0.1% volume fraction, efficiencies attain 0.7496 at 0.0330 kg/s. Conversely, pure water has inferior performance, achieving a maximum. F_r (τα) of 0.558 at 0.0330 kg/s.

Table 4. Performance metrics of SiC NF and water in a solar collector

Solid Volume Fraction	Mass Flow Rate (kg/s)	F_rU_L	F_r (τα)	R²
Water	0.0167	8.0	0.530	0.987
	0.0250	8.232	0.5441	0.9863
	0.0330	8.2875	0.5581	0.9914
0.025%	0.0167	9.2	0.638	0.995
	0.0250	9.531	0.654	0.9936
	0.0330	9.77	0.6751	0.9918
0.05%	0.0167	9.45	0.669	0.992
	0.0250	9.72	0.6825	0.9904
	0.0330	9.915	0.7061	0.989
0.075%	0.0167	9.55	0.682	0.993
	0.0250	9.823	0.6926	0.9936
	0.0330	10.288	0.7259	0.9872
0.1%	0.0167	9.70	0.715	0.991
	0.0250	9.997	0.7268	0.9909
	0.0330	10.382	0.7496	0.9919

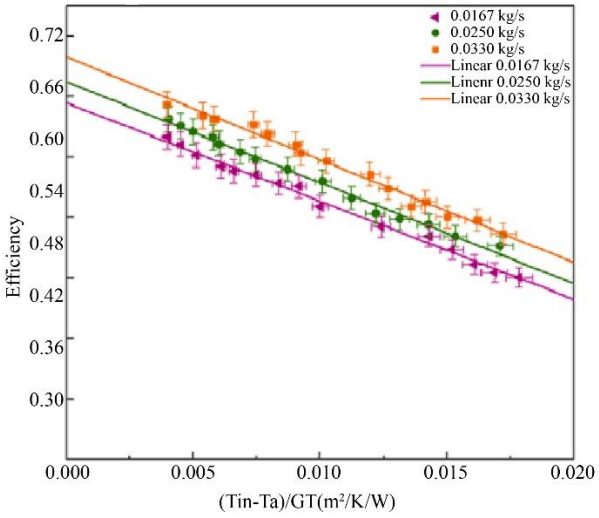

(a) 0.025%

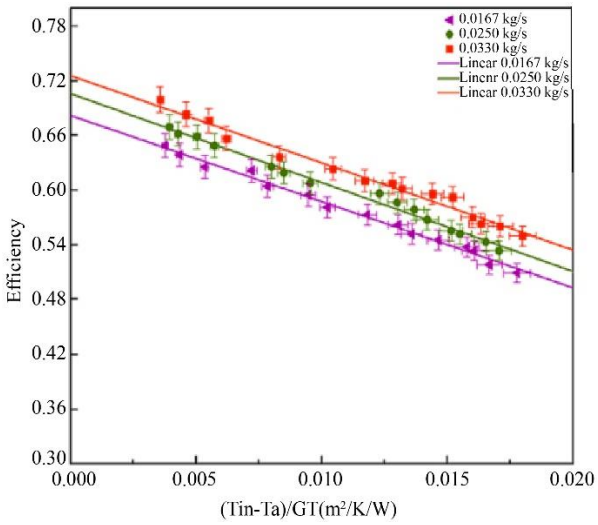

(b) 0.05 %

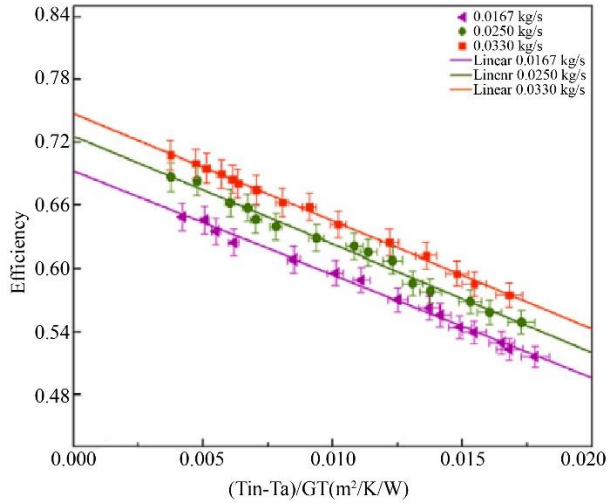

(c) 0.075 %

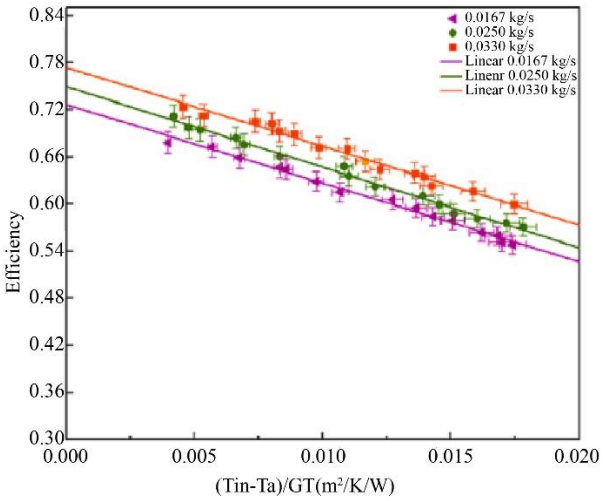

(d) 0.1%

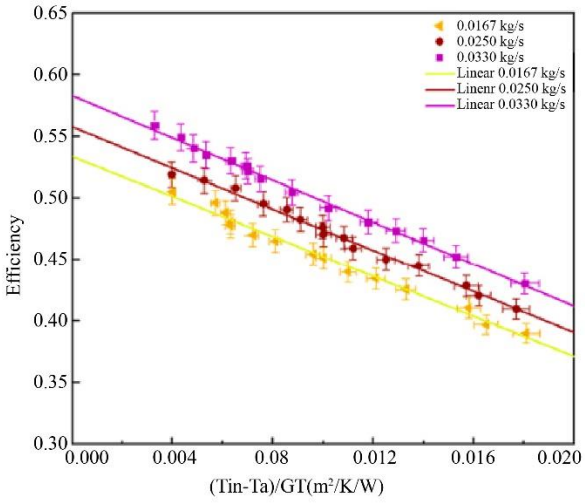

(e) Water

Fig. 12 Impact of the mass flow rate of SiC NF

The outcomes show that using SiC nanoparticles improves the thermo-optical characteristics of the solar collector, underscoring the significance of nanoparticle volume and mass flow rate in performance optimization.

Figure 12 demonstrates the influence of varied mass flow rates on system performance using different volume fractions of SiC and water, focusing on ((Ti-Ta)/GT). Figure 12(a) examines the effect of a 0.025% volume fraction of nanoparticles at various mass flow rates. Figure 12(b) further examines the effects of these mass flow rates at a nanoparticle volume fraction of 0.05%. Figures 12(c) and (d) present the outcomes for volume fractions of 0.075% and 0.1%, respectively. Figure 12(e) displays the outcomes for water over various mass flow rates. A rise in mass flow rate improves both the energy parameter associated with heat removal and the thermo-optical efficiency of the collector.

This improvement provides an elevated Reynolds number at larger flow rates, which increases heat transmission through higher turbulence and improved fluid layer mixing. Brownian motion predominantly influences this effect, which enhances the heat conductivity of NFs relative to water. The findings demonstrate that increased mass flow rates within the examined range result in enhanced efficiency. Therefore, it can be stated that the integration of NFs advances the thermal characteristics of the collector, enabling a greater temperature differential. Therefore, to attain a greater outlet temperature, it is crucial to improve the thermal effectiveness of the collector.

4.5. Performance Comparison

Table 5 demonstrates the performance comparison of different nanoparticles using water as base fluids and the proposed study.

The investigation of thermal conductivity enhancements in various studies reveals substantial gains by incorporating nanoparticles into base fluids. CuO in water produced an 11.3% increase, whereas Al_2O_3 and CNC resulted in an 8.46% boost, illustrating the potential of different NFs. Diamond nanoparticles demonstrated a 12.2% enhancement, highlighting their remarkable thermal characteristics. Functionalized graphene nanoplatelets demonstrated the most remarkable outcome, with a 17.45% improvement, highlighting their superior efficiency. The Al_2O_3 and TiO_2 hybrid system yielded an 8.25% enhancement, signifying moderate success. The suggested study involving SiC nanoparticles indicates continuous progress in NF technology for improved thermal performance.

Table 5. Comparison of thermal conductivity enhancement

Author	Nanoparticle Composition	Base Fluid	Concentration	Maximum enhancement in thermal conductivity
Hussein et al. [7]	CuO	Water	1%	11.3%
Farhana et al. [8]	Al_2O_3, CNC	Water	0.5%	8.46% (CNC)
Zarda et al. [10]	diamond	Water	1%	12.2%
Akram et al. [11]	f-GNPs, ZnO, SiO_2	Distilled water	0.1%	17.45% (f-GNPs)
Bharadwaj [12]	$Al_2O_3 + TiO_2$	Demineralized water	0.75%	8.25%
Proposed study	**SiC**	**Water**	**0.1%**	**31.3%**

5. Conclusion

This study demonstrated the significant advantages of using SiC nanofluids to improve the thermal efficiency of FPSCs. Experimental results confirmed substantial enhancements in heat transfer properties and thermal conductivity, with a peak efficiency of 0.7496 at a 0.1% volume fraction and a mass flow rate of 0.033 kg/s. Characterization techniques such as FTIR, XRD, and TEM validated the structural integrity and stability of the nanofluids, ensuring their reliability for solar thermal applications. The findings suggest that SiC nanofluids can play a crucial role in optimizing solar energy systems by allowing higher heat absorption and energy conversion rates. Beyond efficiency improvements, these results have broader implications for the design of compact and high-performance solar collectors, making them more suitable for industrial heating and power generation. Integrating SiC nanofluids into hybrid solar-thermal systems presents an opportunity for further performance optimization. However, challenges remain regarding long-term stability, nanoparticle dispersion, and scalability. Future research should focus on developing hybrid nanofluids, refining synthesis techniques, and addressing environmental concerns related to nanoparticle production and disposal. Advancements in these areas will contribute to more sustainable and efficient solar thermal technologies, reinforcing the transition to cleaner and more renewable energy solutions.

Acknowledgements

I sincerely thank everyone who contributed to the completion of this research paper. I extend my heartfelt gratitude to my supervisor, family, colleagues, and fellow researchers for their unwavering support, encouragement, and understanding throughout the challenging phases of this work.

References

[1] M.A. Islam et al., *Chapter 5 - Energy Demand Forecasting*, Energy for Sustainable Development: Demand, Supply, Conversion and Management, Academic Press, pp. 105-123, 2020. [CrossRef] [Google Scholar] [Publisher Link]

[2] Biomass Energy, "Renewable Energy sources," *Ergon Energy*, pp. 1-10, 2015. [Google Scholar] [Publisher Link]

[3] Y. Tian, and C.Y. Zhao, "A Review of Solar Collectors and Thermal Energy Storage in Solar Thermal Applications," *Applied Energy*, vol. 104, pp. 538-553, 2013. [CrossRef] [Google Scholar] [Publisher Link]

[4] Fabio Struckmann, "*Analysis of a Flat-Plate Solar Collector*," MVK160 Heat and Mass Transport, Project Report, Lund University, Lund, Sweden, pp. 1-4, 2008. [Google Scholar]

[5] Himangshu Bhowmik, and Ruhul Amin, "Efficiency Improvement of Flat Plate Solar Collector using Reflector," *Energy Reports*, vol. 3, pp. 119-123, 2017. [CrossRef] [Google Scholar] [Publisher Link]

[6] Yang Li et al., "Investigation on Heat Transfer Performances of Nanofluids in Solar Collector," *Materials Science Forum*, vol. 694, pp. 33-36, 2011. [CrossRef] [Google Scholar] [Publisher Link]

[7] Adnan M. Husseın, Afrah Turki Awad, and Hussein Hayder Mohammed Ali, "Evaluation of the Thermal Efficiency of Nanofluid Flows in Flat Plate Solar Collector," *Journal of Thermal Engineering*, vol. 10, no. 2, pp. 299-307, 2024. [Google Scholar] [Publisher Link]

[8] K. Farhana et al., "Analysis of Efficiency Enhancement of Flat Plate Solar Collector Using Crystal Nano-Cellulose (CNC) Nanofluids," *Sustainable Energy Technologies and Assessments*, vol. 45, 2021. [CrossRef] [Google Scholar] [Publisher Link]

[9] A.A. Hawwash et al., "Thermal Analysis of Flat Plate Solar Collector Using Different Nanofluids and Nanrticles Percentages," *IEEE Access*, vol. 9, pp. 52053-52066, 2021. [CrossRef] [Google Scholar] [Publisher Link]

[10] Falah Zarda et al., "Enhancement of Thermal Efficiency of NF Flows in a Flat Solar Collector Using CFD," *Diagnostyka*, vol. 23, no. 4, pp. 1-9, 2022. [CrossRef] [Google Scholar] [Publisher Link]

[11] Naveed Akram et al., "Experimental Investigations of the Performance of a Flat-Plate Solar Collector using Carbon and Metal Oxides Based Nanofluids," *Energy*, vol. 227, 2021. [CrossRef] [Google Scholar] [Publisher Link]

[12] Gaurav Bharadwaj, "Performance Analysis of FPSC Using Hybrid Nanofluid of Aluminum Oxide and Titanium Oxide," *IOP Conference Series: Materials Science and Engineering: International Conference on Futuristic and Sustainable Aspects in Engineering and Technology*, Mathura, India, vol. 1116, pp. 1-6, 2021. [Google Scholar] [Publisher Link]

[13] Seyed Pooya Aghili Yegane, and Alibakhsh Kasaeian, "Thermal Performance Assessment of a Flat-Plate Solar Collector Considering Porous Media, Hybrid Nanofluid and Magnetic Field Effects," *Journal of Thermal Analysis and Calorimetry*, vol. 141, pp. 1969-1980, 2020. [CrossRef] [Google Scholar] [Publisher Link]

[14] Nagesh Babu Balam et al., Higher Order Accurate Transient Numerical Model to Evaluate the Natural Convection Heat Transfer in Flat Plate Solar Collector," *Processes*, vol. 9, no. 9, pp. 1-16, 2021. [CrossRef] [Google Scholar] [Publisher Link]

[15] Mehak Shafiq et al., "Thermo-Hydraulic Performance Analysis of Fe_3O_4-Water Nanofluid-Based Flat-Plate Solar Collectors," *Sustainability*, vol. 15, no. 6, pp. 1-21, 2023. [CrossRef] [Google Scholar] [Publisher Link]

[16] Ahmed M. Ajeena, Istvan Farkas, and Piroska Vig, "Performance Enhancement of Flat Plate Solar Collector Using ZrO_2-SiC/DW Hybrid Nanofluid: A Comprehensive Experimental Study," *Energy Conversion and Management: X*, vol. 20, pp. 1-29, 2023. [CrossRef] [Google Scholar] [Publisher Link]

[17] Yi He et al., "Thermal Performance and Experimental Analysis of Stainless Steel Flat Plate Solar Collector with Full-Flow Channels," *Heliyon*, vol. 10, no. 7, pp. 1-14, 2024. [CrossRef] [Google Scholar] [Publisher Link]

[18] May M. Eid, *Characterization of Nanoparticles by FTIR and FTIR-Microscopy*, Handbook of Consumer Nanoproducts, Springer International Publishing, pp. 1-30, 2022. [CrossRef] [Google Scholar] [Publisher Link]

[19] Rajesh Sardar, and Jennifer S. Shumaker-Parry, "Spectroscopic and Microscopic Investigation of Gold Nanoparticle Formation: Ligand and Temperature Effects on Rate and Particle Size," *Journal of the American Chemical Society*, vol. 133, no. 21, pp. 8179-8190, 2011. [CrossRef] [Google Scholar] [Publisher Link]

[20] Ramin Ranjbarzadeh, and Raoudha Chaabane, "Experimental Study of Thermal Properties and Dynamic Viscosity of Graphene Oxide/Oil Nano-Lubricant," *Energies*, vol. 14, no. 10, pp. 1-16, 2021. [CrossRef] [Google Scholar] [Publisher Link]

[21] N. Ben Khedher, "Experimental Evaluation of a Flat Plate Solar Collector Under Hail City Climate," *Engineering, Technology & Applied Science Research*, vol. 8, no. 2, pp. 2750-2754, 2018. [CrossRef] [Google Scholar] [Publisher Link]